ADVANCED FUNCTIONAL MATERIALS
www.afm-journal.de

Antifreezing Hydrogel with High Zinc Reversibility for Flexible and Durable Aqueous Batteries by Cooperative Hydrated Cations

Minshen Zhu, Xiaojie Wang, Hongmei Tang, Jiawei Wang, Qi Hao, Lixiang Liu, Yang Li, Kai Zhang, and Oliver G. Schmidt*

Hydrogels are widely used in flexible aqueous batteries due to their liquid-like ion transportation abilities and solid-like mechanical properties. Their potential applications in flexible and wearable electronics introduce a fundamental challenge: how to lower the freezing point of hydrogels to preserve these merits without sacrificing hydrogels' basic advantages in low cost and high safety. Moreover, zinc as an ideal anode in aqueous batteries suffers from low reversibility because of the formation of insulative byproducts, which is mainly caused by hydrogen evolution via extensive hydration of zinc ions. This, in principle, requires the suppression of hydration, which induces an undesirable increase in the freezing point of hydrogels. Here, it is demonstrated that cooperatively hydrated cations, zinc and lithium ions in hydrogels, are very effective in addressing the above challenges. This simple but unique hydrogel not only enables a 98% capacity retention upon cooling down to –20 °C from room temperature but also allows a near 100% capacity retention with >99.5% Coulombic efficiency over 500 cycles at –20 °C. In addition, the strengthened mechanical properties of the hydrogel under subzero temperatures result in excellent durability under various harsh deformations after the freezing process.

1. Introduction

Rapid development of flexible and wearable electronics has driven the development of rechargeable flexible batteries with better safety and higher durability while maintaining the high energy density.[1] Batteries that employ non-aqueous electrolyte, particularly lithium ion batteries, evoke serious safety concerns due to the usage of flammable electrolytes.[2,3] On the other hand, aqueous batteries have emerged as promising candidates because of good energy density and intrinsically high safety.[4] In addition to the safety, durability is another essential attribute that should be achieved by flexible batteries. While it is extremely difficult to realize high durability for flexible lithium ion batteries owing to the stringent operational environment, using hydrogels as quasi-solid-state aqueous electrolytes straightforwardly endows remarkable durability for flexible aqueous batteries.[5–9] Crosslinked networks of hydrophilic polymer chains dispersed in water provides the hydrogel with solid-like mechanical properties with on-demand design of toughness and elasticity to tolerate even severe and long-lasting mechanical deformations. Meanwhile, the water-rich structure makes hydrogels behave like liquid, which enables fast ion transportation. Ionic conductivity and electrochemical activity are durable as long as the liquid-like property is preserved.[10–13] However, hydrogels lose these desirable properties once the temperature decreases below the

Dr. M. Zhu, H. Tang, Dr. J. Wang, Prof. Q. Hao, L. Liu, Y. Li, Prof. O. G. Schmidt
Institute for Integrative Nanosciences
IFW Dresden
01069 Dresden, Germany
E-mail: m.zhu@ifw-dresden.de

X. Wang, Prof. K. Zhang
Wood Technology and Wood Chemistry
Georg-August-Universität Göttingen
37077 Göttingen, Germany

The ORCID identification number(s) for the author(s) of this article can be found under https://doi.org/10.1002/adfm.201907218.

DOI: 10.1002/adfm.201907218

H. Tang, Dr. J. Wang, L. Liu, Y. Li, Prof. O. G. Schmidt
Materials Systems for Nanoelectronics
TU Chemnitz
09107 Chemnitz, Germany

Dr. J. Wang, Prof. O. G. Schmidt
Center for Materials
Architectures and Integration of Nanomembranes
TU Chemnitz
09126 Chemnitz, Germany

Prof. Q. Hao
School of Physics
Southeast University
211189 Nanjing, P. R. China

Prof. O. G. Schmidt
Nanophysics
Faculty of Physics
TU Dresden
01062 Dresden, Germany

freezing point of water, whereas the working temperature of flexible and wearable electronics is supposed to extend to subzero temperatures. Therefore, freezing severely limits the practicability of flexible batteries using hydrogels as the electrolyte, especially under subzero temperatures.

One strategy to design antifreezing hydrogels is incorporating organic liquids to synthesize hybrid organohydrogels.[14,15] The organogel components can efficiently inhibit the formation of ice crystals. However, concerns about health hazard as a result of toxicity of organic liquids are raised especially regarding the safety issue for flexible and wearable electronics. On the other hand, freezing tolerance also derives from the colligative property of concentrated solutions containing ionic compounds, which can suppress ice crystallization in water due to ion hydration. This freezing-point depression is a well-known phenomenon with many examples in nature and in our daily life. For example, antifreezing seawater is the result of the mixture of salts in water. Chloride salts are widely used to prevent roads from icing under subzero temperatures. Moreover, the chloride salts have been successfully applied in antifreezing hydrogels used for wearable and flexible sensors, which have shown excellent conductivity and mechanical durability under subzero temperatures.[16] Meanwhile, ionic compounds that strongly interact with water molecules, such as lithium chloride and zinc sulfate, are intrinsically involved in the electrolyte system for aqueous batteries. Therefore, it would be not surprising if the freezing point of the aqueous phase in the hydrogel electrolyte can be facilely and directly lowered by tuning the hydration in hydrogels. However, such a simple and straightforward approach has not been thoroughly investigated to design hydrogels under subzero temperatures for flexible aqueous batteries.

In terms of aqueous batteries, metallic zinc (Zn) is an ideal anode material due to its high theoretical capacity, low electrochemical potential, high abundance, and low toxicity.[17–21] The reaction takes place at the Zn anode and can be regarded as a typical plating–stripping process. Generally, hydrogen evolution also occurs during the deposition of Zn, leading to the pH rise in the vicinity of plated Zn. As a result, $Zn(OH)_2$, ZnO, and zincates are likely to form during plating–stripping cycles.[22–25] Consequently, the irreversibility issue arises due to the formation of these insulative byproducts. Moreover, concentrated divalent Zn ions in electrolyte for aqueous batteries aggravates the irreversibility issue because they are strongly hydrated with water molecules. Therefore, the suppression of the hydration of Zn^{2+} is regarded as an effective strategy to improve the durability of the Zn anode more significantly, and the aim of hydration suppression conflicts with the purpose to lower the freezing point of the hydrogel, which creates a dilemma to design an ideal hydrogel that meets both requirements. Alternatively, concepts of "water in salt" that restrain the hydrogen evolution by special anions and the utilization of zinc molten hydrate that minimizes the water content have been developed and show impressive results.[26–28] However, costly salts used in "water in salt" and incompatibility with hydrogels of the zinc molten hydrate compromise any benefits anticipated for hydrogel based aqueous batteries in practical applications, such as low cost and excellent mechanical durability.

Here, we report about a simple polyacrylamide hydrogel (PAAm) consisting of cooperative cations, 2 mol L^{-1} $ZnSO_4$ and 4 mol L^{-1} LiCl. Highly hydrated cations not only lower the freezing temperature of the hydrogel but also improve the reversibility of the zinc anode cycled in the hydrogel. The former attribute gives rise to an excellent capacity retention (98%) achieved by the flexible aqueous battery based on $LiFePO_4$ and Zn upon cooling down to −20 °C from room temperature, as well as the outstanding durability under various mechanical deformations over a wide temperature range. The latter advantage enables a highly stable cycling performance, almost 100% retention at >99.5% Coulombic efficiency over 500 cycles at −20 °C. The spectroscopic and structural investigations reveal that the mixture cations, zinc (Zn^{2+}) and lithium ions (Li^+), cooperatively dissociate the intermolecular hydrogen bonding between water molecules by the cooperative hydration, which significantly reduces the freezing temperature of the hydrogel.[29] Consequently, high ion transportation and solid-like mechanical properties are maintained under subzero temperatures. In addition, cooperated by preferable adsorption of the supporting cation, Li^+, the underpotential hydrogen evolution is suppressed and so does the formation of $Zn(OH)_2$ and ZnO. As a result, the highly reversible zinc anode in the hydrogel is achieved. The disclosed fundamental roles of cooperative hydrated cations in the hydrogel's physical and electrochemical properties and demonstration of a highly durable and flexible aqueous battery under subzero temperatures will open up a new avenue to versatile hydrogels for advanced flexible aqueous batteries with low cost, high safety, high stability, and durable mechanical properties in a wide working temperature range, which are imperatively needed for flexible and wearable electronics.

2. Results and Discussion

The hydrogel is prepared from the mixture solution containing acrylamide monomers and specific salts. Ammonium persulfate (APS) and *N*,*N*′-methylenebis(acrylamide) are dissolved into the solution as initiator and crosslinker, respectively. The free radical polymerization is initiated at 70 °C (**Figure 1**a). Transparent hydrogels after polymerization are shown in Figure S1 (Supporting Information). Dissolved ions in hydrogels substantially modify the structure and dynamics of water molecules due to the hydration. The structure of the water molecules is revealed by the Raman spectra in Figure 1b.[30] We identify two main contributions to the water vibration band of the pure PAAm: intermolecular hydrogen bonds at 3220 cm^{-1} and asymmetric stretching at 3420 cm^{-1}.[31,32] In general, hydrated ions in water diminish the intermolecular hydrogen bonds and elevate the asymmetric stretching. Typically, ions with a larger charge density (small, multivalent ions) have higher hydration numbers than ions with a lower charge density (large, monovalent ions), thus affecting the structure of a larger number of water molecules. As a result, the addition of commonly used electrolyte, 2 mol L^{-1} $ZnSO_4$, into the PAAm hydrogel (referred to as Z-PAAm hereafter) significantly reduces the contribution from intermolecular hydrogen bonding due to two strongly hydrated ions (Zn^{2+} and SO_4^{2-}). However, the strong ion pairing between Zn^{2+} and SO_4^{2-} that induces the aggregation of ions alleviates the hydration.[33–35] This is supported by

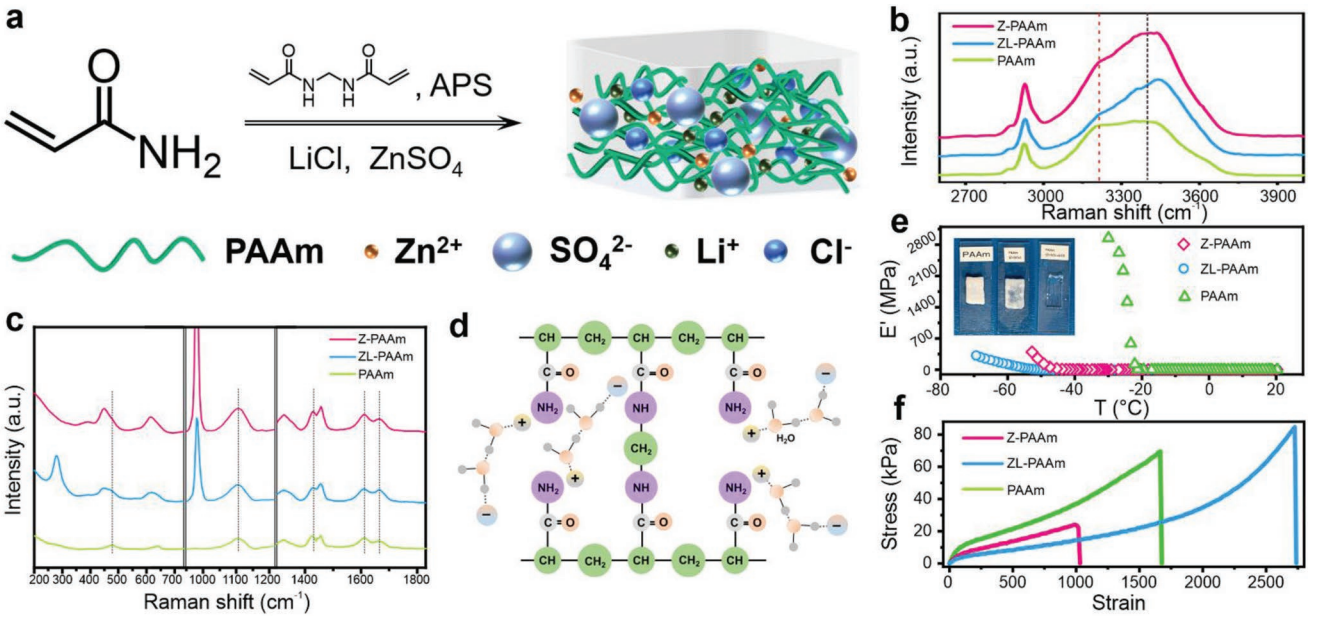

Figure 1. a) Schematic illustration of synthesis of the hydrogel. b,c) Raman spectra of the PAAm, Z-PAAm, and ZL-PAAm in specific ranges. d) Chemical structure of the ZL-PAAm. e) Temperature dependence of the storage modulus and f) stress–strain curves of the hydrogels.

the fact that the reduction of intermolecular hydrogen bonds and enhancement of asymmetric stretching of Z-PAAm is less obvious than PAAm containing 2 mol L^{-1} $ZnCl_2$ (Figure S2a, Supporting Information), even though the hydration number of Cl^- is negligible in water.[36] Therefore, in order to further intensify the hydration of water in hydrogels, adding alternative ions with high hydration number is a more efficient strategy than pushing the concentration of $ZnSO_4$. Considering the compatibility with aqueous batteries, lithium salts are preferable choices. Owing to the relatively low solubility, the addition of Li_2SO_4, rather than enhancing the hydration, impedes the association with water molecules due to the aggregation of strongly bonded ion pairs (Figure S2b, Supporting Information). Therefore, LiCl (4 mol L^{-1}), a highly soluble salt containing highly hydrated Li^+ ion, is introduced, forming a mixture solution containing Li^+, Zn^{2-}, Cl^-, and SO_4^{2-} ions. The high solubility of chlorides can effectively prevent ion aggregation, thus ensuring hydration of Li^+, Zn^{2-}, and SO_4^{2-} even at a high concentration. As expected, after adding 2 mol L^{-1} $ZnSO_4$ and 4 mol L^{-1} LiCl into PAAm (referred to as ZL-PAAm hereafter), the contribution from intermolecular hydrogen bonds is further reduced, whereas the contribution from asymmetric stretching increases and shifts to a higher frequency. This indicates more water molecules are bonded to the ions.[32,37] The higher level of hydration raised by hybrid ions is further supported by the lower pH of the mixture solution ($ZnSO_4$ and LiCl) compared to pure $ZnSO_4$ solution (Figure S3a, Supporting Information). Furthermore, the OH^- produced by the highly hydrated SO_4^{2-} will interact with H^+, thus increasing the relative ratio between H^+ and OH^- and leading to a decrease of the pH value.[38] However, the higher hydration level of 2 mol L^{-1} $ZnCl_2$ solution than that of 2 mol L^{-1} $ZnSO_4$ solution indicates the severe aggregation of the $ZnSO_4$ (Figure S3b, Supporting Information). However, the addition of LiCl alleviates the aggregation of $ZnSO_4$ in a high concentration. As a result, cooperative hydration anions (SO_4^{2-}) enhance the hydration level of the mixture solution.

Figure 1c shows the Raman spectra of the vibrations from polymer chains in PAAm, Z-PAAm, and ZL-PAAm. The vibration bands at 1664, 1610, and 1425 cm^{-1} (right panel) in PAAm are assigned to C–O stretching (amide I), NH_2 bending (amide II), and C–N stretching (amide III), respectively.[39] For the PAAm containing salts, three amide vibrations are observed at the same frequency, indicating that the main structures of PAAm, Z-PAAm, and ZL-PAAm are identical. However, the hydrogen bonding between NH_2 groups in ZL-PAAm is weakened as shown by the decrease in relative intensity of the amide II vibration (right panel, Figure 1c), indicating the regularity of NH_2 groups is impaired (Figure S4a, Supporting Information). Moreover, the increase in full width at half-maximum (FWHM) further confirms the reduction of the regularity NH_2 groups (Figure S4b, Supporting Information), which is ascribed to the circumstance that Li^+ functions as a "pseudoprotonic acid" dopant that can displace interchain hydrogen bonding.[40] The reduced hydrogen bonding in ZL-PAAm is further supported by the decrease in storage modulus (Figure S5, Supporting Information). Characteristic peaks of C–C skeletal stretching (middle panel) for three hydrogels all locate at 1105 cm^{-1}, further confirming the main structure of PAAm is not altered by hydrated ions.[41] However, the decrease in frequency of the peaks corresponding to the C–C deformation (450 cm^{-1}, left panel) is observed for Z-PAAm and ZL-PAAm, showing that more skeletal deformation is introduced along with the addition of salts. The increased deformation is most likely due to the strongly hydrated SO_4^{2-}, which presumably forms hydrogen bonds to NH_2 groups.[42] This is confirmed by the stable frequency of the C–C deformation when adding LiCl and $ZnCl_2$ into PAAm (Figure S6a, Supporting Information) and exacerbated deformation in the mixture solution of $ZnSO_4$ and

Li_2SO_4 (Figure S6b, Supporting Information). Figure S6c (Supporting Information) shows the C–C deformation band and the C–C skeletal band with different components. The intensity ratio between the C–C deformation band and the C–C skeletal band is summarized in Figure S6d (Supporting Information). Obviously, the intensity ratio of the C–C deformation band in the Z-PAAm is more significant than that of the ZL-PAAm, which indicates the deformation degree of the C–C skeleton of Z-PAAm is more pronounced than that of the ZL-PAAm.[41] In contrast, the deformation is not exacerbated by adding the salts without SO_4^{2-}. Therefore, the deformation is attributed to the hydrogen bonding between SO_4^{2-} and NH_2 groups in polymer chains. Owing to the strong ion pairing between additional Li^+ and SO_4^{2-}, SO_4^{2-} will be partially confined by the Li^+. Therefore, the reduced structural deformation of ZL-PAAm is attributed to the alleviated formation of hydrogen bonding between SO_4^{2-} and NH_2 groups due to the pairing between Li^+ and SO_4^{2-}. However, although the structure regularity will be better if replacing $ZnSO_4$ by $ZnCl_2$, the inferior zinc reversibility of $ZnCl_2$ (Figure S7, Supporting Information) will reduce the practicability of the hydrogel in aqueous batteries based on the zinc anode. Figure 1d schematically illustrates the structure of ZL-PAAm, which suggests two attributes of the PAAm chains with the addition of Li^+. 1) Li^+ ions function as cooperative ions to enhance the hydration level, which is beneficial for lowering the freezing point. 2) Li^+ ions reduce interchain hydrogen bonding in ZL-PAAm due to the doping effect, which may improve the strain tolerance. Meanwhile, Li^+ ions prevent the severe distortion of polymer chains through the ion pairing with SO_4^{2-}, which ensures the mechanical durability of the hydrogel.

Figure 1e shows the increase in storage modulus of hydrogels when the temperature reaches the freezing point, indicating the hydrogel becomes brittle due to the icing of the aqueous phase. As expected, the freezing point decreases with the addition of salts into PAAm. The ZL-PAAm shows the lowest freezing point of the three hydrogels, enabling the widest temperature range with stable mechanical properties. Specifically, transition temperatures of PAAm, Z-PAAm, and ZL-PAAm are −15, −30, and −45 °C, respectively (Figure S8, Supporting Information). As shown by the inset in Figure 1e, the ZL-PAAm does not freeze after the storage at −20 °C for 10 min. By contrast, PAAm totally freezes into a brittle solid and Z-PAAm starts to freeze. The stress–strain curves of hydrogels are shown in Figure 1f. Owing to the distortion of the polymer chains, the Z-PAAm shows the worst mechanical properties among the three hydrogels and withstands the smallest strain and fracture stress. Interestingly, compared to PAAm, larger strain can be applied to the ZL-PAAm before fracture. This is caused by the enhanced mobility of the polymer chains due to the reduced hydrogen bonding between polymer chains via the addition of LiCl. Meanwhile, a slight improvement of fracture stress at the expense of elasticity is observed for ZL-PAAm. This is ascribed to the increase in internal friction caused by chain slipping due to the lack of interchain hydrogen bonding, which dissipates more energy upon deformation. All in all, the ZL-PAAm shows an ultralow freezing point and excellent mechanical durability due to the introduction of highly hydrated Li^+ and Zn^{2+} into the hydrogel.

Nyquist plots of hydrogels sandwiched by two blocking electrodes are recorded at different temperatures to derive the ionic conductivities (Figure S9, Supporting Information), which are temperature dependent as shown in **Figure 2**a.[43,44] Generally, ionic conductivity decreases upon cooling. Two regions split by 0 °C can be identified for Z-PAAm and ZL-PAAm: slow decrease of ionic conductivity in the temperature range above

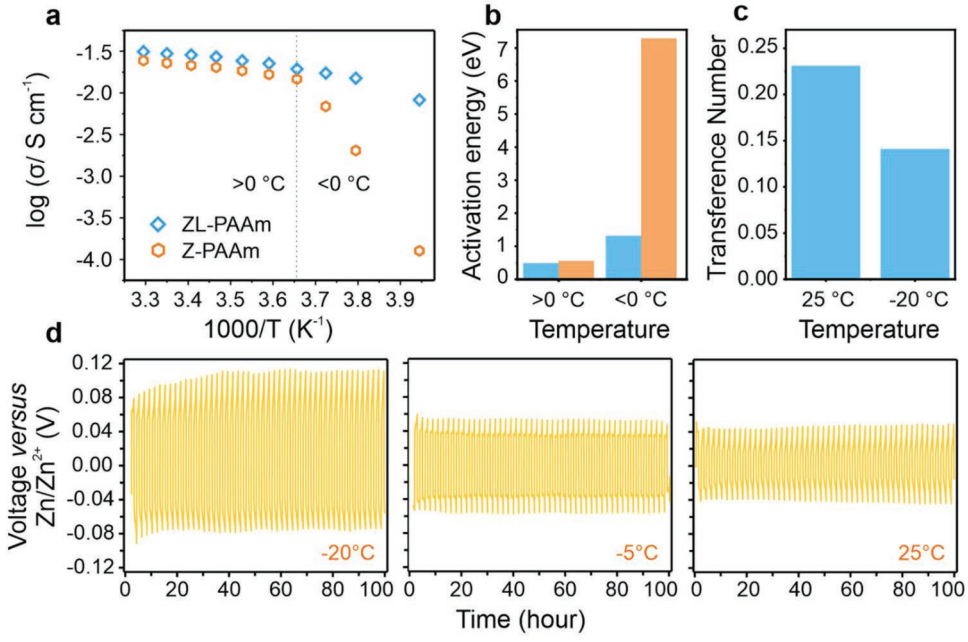

Figure 2. a) Variation in conductivity with temperature. b) Activation energy derived from the Arrhenius plot of conductivity at >0 and <0 °C of Z-PAAm (blue column) and ZL-PAAm (orange column). c) Zn transference number of ZL-PAAm at different temperatures. d) The voltage profiles of Zn plating–stripping in ZL-PAAm under different temperatures.

0 °C and fast decay when the temperature is cooled down to below 0 °C. Interestingly, although freezing points of both hydrogels are far below 0 °C, the ZL-PAAm shows a remarkably better ionic conductivity than Z-PAAm at subzero temperatures. Moreover, the addition of pure LiCl does not maintain the high ionic conductivity at –20 °C (Figure S10a, Supporting Information), letting alone the huge hindrance for the reversibility zinc deposition (Figure S10b, Supporting Information). Therefore, the high performance at subzero temperatures of ZL-PAAm is attributed to the synergy functions from ions in the hydrogel. The ionic conductivity of Z-PAAm dramatically decreases whereas it decays gently for ZL-PAAm below 0 °C. As is known, the ionic conductivity depends on the number of dissociated ions. At subzero temperature, it needs more energy to dissociate enough ion pairs due to the recombination of ion pairs caused by dehydration. Therefore, along with the lowering level of hydration, the higher activation energy is observed for ion transportation. Accordingly, Figure 2b shows dramatically increased activation energy (from 0.55 to 7.29 eV) of Z-PAAm at subzero temperatures due to the relatively low level of hydration. On the other hand, the activation energy remains small for ZL-PAAm due to the assisted hydration by Li^+. Ion transportation of ZL-PAAm at 25 and –20 °C is further investigated by recording the variation of current and impedance with time before and after polarization (Figure S11, Supporting Information).[43,45] The calculated ion transference numbers are shown in Figure 2c. The value moderately decreases from 0.23 to 0.14 when the temperature cools down from 25 to –20 °C, which further confirms the high ion transportation at subzero temperatures in ZL-PAAm. In addition to the ion transport in ZL-PAAm, symmetric cells of Zn/Zn are assembled and cycled at 1 mA cm^{-2} for 1 mAh cm^{-2}. Figure 2d shows the voltage profiles of 100 plating–stripping cycles at different temperatures. In accordance with the reduced ionic conductivity at –20 °C, the mass-transfer controlled potential (μ_{mtc}) is larger than that at higher temperatures. The difference between μ_{mtc} at –5 and 25 °C is very small, demonstrating a wide temperature range with high ion migration abilities. Moreover, the voltage profiles at different temperatures exhibit excellent potential retention upon cycling, which points to a highly reversible Zn anode based on ZL-PAAm hydrogel.

In **Figure 3**a, we compare the μ_{mtc} of Zn/Zn symmetric cells based on ZL-PAAm and Z-PAAm at 1 mA cm^{-2} for 1 mAh cm^{-2}. A relatively small μ_{mtc} (80 mV) and stable potential

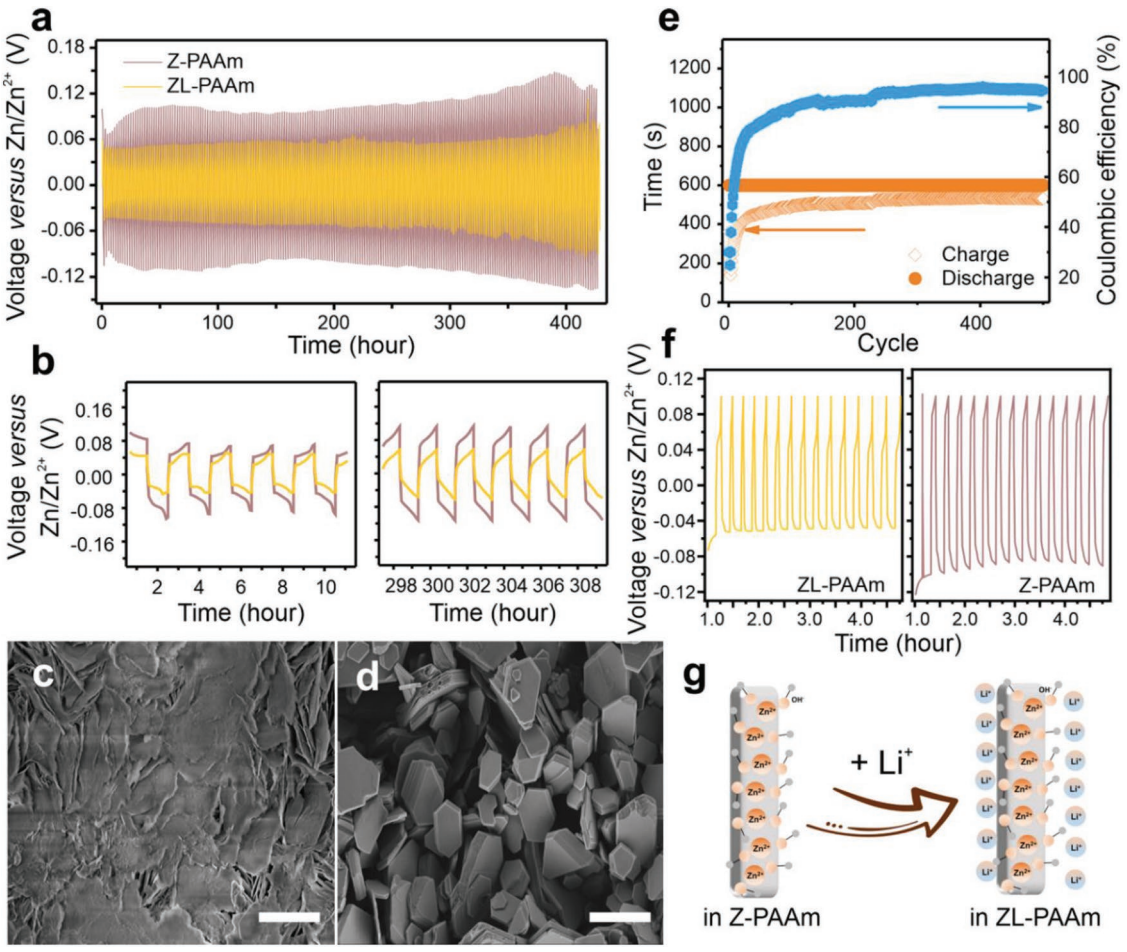

Figure 3. a) Voltage profiles of Zn plating–stripping in Z-PAAm and ZL-PAAm and b) magnified profiles in 1–10 and 297–309 h. SEM images of the Zn foil cycled in c) Z-PAAm and d) ZL-PAAm (scale bar: 4 µm). e) The Coulombic efficiency and f) magnified voltage profiles of Zn plating–stripping in the asymmetric cell of ZL-PAAm. g) Schematic illustration of the interfacial reactivity in Z-PAAm and ZL-PAAm.

retention over 400-hour cycling explains that Z-PAAm is widely used in flexible aqueous batteries. Nevertheless, a smaller μ_{mtc} is observed for ZL-PAAm, indicating a lower interfacial impedance than Z-PAAm. Magnified voltage profiles in Figure 3a for the time range of 1–10 and 297–309 h are displayed in Figure 3b. Initially, the difference in μ_{mtc} between Z-PAAm and ZL-PAAm is relatively small. Along with cycling, μ_{mtc} starts to overshoot for Z-PAAm, whereas μ_{mtc} of ZL-PAAm remains at small value. This difference lies in the product after cycling Zn in hydrogels. As expected, insulative $Zn(OH)_2$ and ZnO, in addition to the Zn, are identified by the X-ray diffraction (XRD) patterns for the zinc foil cycled in Z-PAAm (Figure S12a, Supporting Information). Such insulating layer formed on the surface of the Zn foil increases the resistance, resulting in the increased μ_{mtc}. In sharp contrast, only Zn and residual lithium salts are detected for the ZL-PAAm (Figure S12b, Supporting Information), which preserve the high conductivity of the Zn foil cycled in ZL-PAAm. Thus, the low μ_{mtc} is stable throughout the cycling test. The absence of $Zn(OH)_2$ and ZnO in ZL-PAAm suggests an alternative interfacial reaction for plating, in which the hydrogen evolution is substantially suppressed. The detailed mechanism will be discussed below. SEM images of the zinc foil after 400-hour cycling also reveal distinct differences in morphologies of products formed on cycled Zn foils. The cycled zinc foil in Z-PAAm shows a rough surface and a dense structure assembled by irregular nanodisks (Figure 3c). In contrast, oriented growth of hexagonal rods of Zn are observed for the cycled zinc foil in ZL-PAAm (Figure 3d). The preferable growth is attributed to the capping effect of Li^+ on the Zn nuclei.[46–48] In addition, hexagonal nanoparticles randomly form on the zinc foil rather than accumulate into a dense structure. The voids between assemblies create the "porosity" on the surface of zinc foils, which will facilitate the mass transfer and enable low μ_{mtc} over the full length of the cycling.[16]

To gain the fundamental understanding of high reversibility of the zinc anode in hydrogels, asymmetric cells using a platinum (Pt) foil as the working electrode are assembled. During the cycling, Zn is firstly plated onto the Pt foil with a capacity of 0.2 mAh cm^{-2} at 1 mA cm^{-2}, followed by stripping Zn to a cutoff voltage which signifies that all the removable Zn has been stripped from the surface of the Pt foil. The Coulombic efficiency (CE) of ZL-PAAm, calculated from the ratio of Zn stripped from the Pt foil to that platted during the same cycle, is shown in Figure 3e. Remarkably, a stable CE of 95% is maintained for hundreds of cycles, which implies that most Zn deposited on the Pt foil could be recovered in the following stripping process. In contrast, the stable CE of Z-PAAm is 83% (Figure S13, Supporting Information), suggesting the inferior reversibility compared to that of ZL-PAAm. In general, conditioning of the foreign metal, as shown by the gradual increase in CE during the initial cycles, is inevitable when using asymmetric cells.[49] The conditioning introduces unstripped residuals on the Pt foils, which could precisely dictate the interfacial reactivity for the metal deposition.[50] Therefore, Pt foils after the final stripping of removable zinc are characterized by XRD. In accordance with the results from symmetric cells, XRD patterns show Zn and residual lithium salts on the Pt foil cycled in ZL-PAAm (Figure S14a, Supporting Information) whereas $Zn(OH)_2$ and ZnO for Z-PAAm (Figure S14b, Supporting Information). As discussed above, the formation of $Zn(OH)_2$ and ZnO is ascribed to the hydrogen evolution process during plating. Therefore, the absence of these two products in ZL-PAAm points to the suppression of the hydrogen evolution during the plating. However, the deprotonation of water, the main contributor to the hydrogen evolution, is not suppressed as shown by the high acidity of the $ZnSO_4$ solution after adding LiCl (Figure S2a, Supporting Information). Moreover, the bubble formation that may also suppress further hydrogen evolution is not observed during the plating process (Figure S15, Supporting Information). Therefore, it is reasonable to attribute the restraint hydrogen evolution to the inhibiting effect of the supporting cation, Li^+. Figure S16a (Supporting Information) shows the linear sweep voltammetry (LSV) of the acidic solution with Pt as the working electrode, which demonstrates a capacitive behavior in the region of −0.4 to −0.8 V versus saturated calomel electrode (SCE), followed by the direct hydrogen evolution.[10] The inset in Figure S16a (Supporting Information) shows the LSV curves of pure LiCl solution with different concentrations. We can also observe the capacitive behavior when the potential decreases to below 0 V, indicating the adsorption of the cations and the establishment of the electric double layer. As Li^+ interacts with water molecules, the resistance to establish the electric double layer is higher at a higher concentration.[26] Therefore, the interaction between water molecules and Li^+ affects capacitive behavior. At a high hydrolysis level, more water molecules will interact with Li^+. As a result, we observe an obvious peak, which corresponds to the dissociation of Li^+ with water molecules and the subsequent establishment of the electric double layer through a capacitive behavior. In contrast, this peak is absent for the solution without LiCl while the underpotential hydrogen evolution is detected (Figure S16b, Supporting Information).[51] Consistent with the LSV result, cyclic voltammetry (CV) demonstrates the adsorption of Li^+ ions significantly facilitate the deposition of Zn in ZL-PAAm by suppressing the underpotential hydrogen evolution (Figure S17a, Supporting Information) while underpotential hydrogen evolution occurs together with the zinc deposition in Z-PAAm (Figure S17b, Supporting Information).[52] As a result, the conversion to insulative products from deposited Zn due to the hydrogen evolution is largely prohibited via the addition of LiCl. In addition, the stage of $Zn(OH)_2$ formation is shown in voltage profiles (1 to 15th plating and stripping cycles) of asymmetric cells based on Z-PAAm and ZL-PAAm (Figure 3f). The near zero capacity for the first stripping implies that $Zn(OH)_2$ is abundantly formed. This is further supported by the abnormal voltage profile of the second plating, which is related to the deposition of Zn via $Zn(OH)_2$ layer.[53] Such reduction reaction is also responsible for the initial decrease in μ_{mtc} of the symmetric cell based on Z-PAAm as shown in Figure 3a, where the conditioned $Zn(OH)_2$ is continuously reduced to Zn. In sharp contrast, the first Coulombic efficiency of ZL-PAAm reaches 64%, further confirming the $Zn(OH)_2$ formation is restricted. Owing to the unremovable layer of $Zn(OH)_2$, the μ_{mtc} of Z-PAAm in either the symmetric or asymmetric cell is almost twice that of ZL-PAAm. In summary, the addition of supporting hydrated cations, Li^+, establishes a new interface between the anode and electrolyte (Figure 3g). Following the adsorption of Zn^{2+} on the

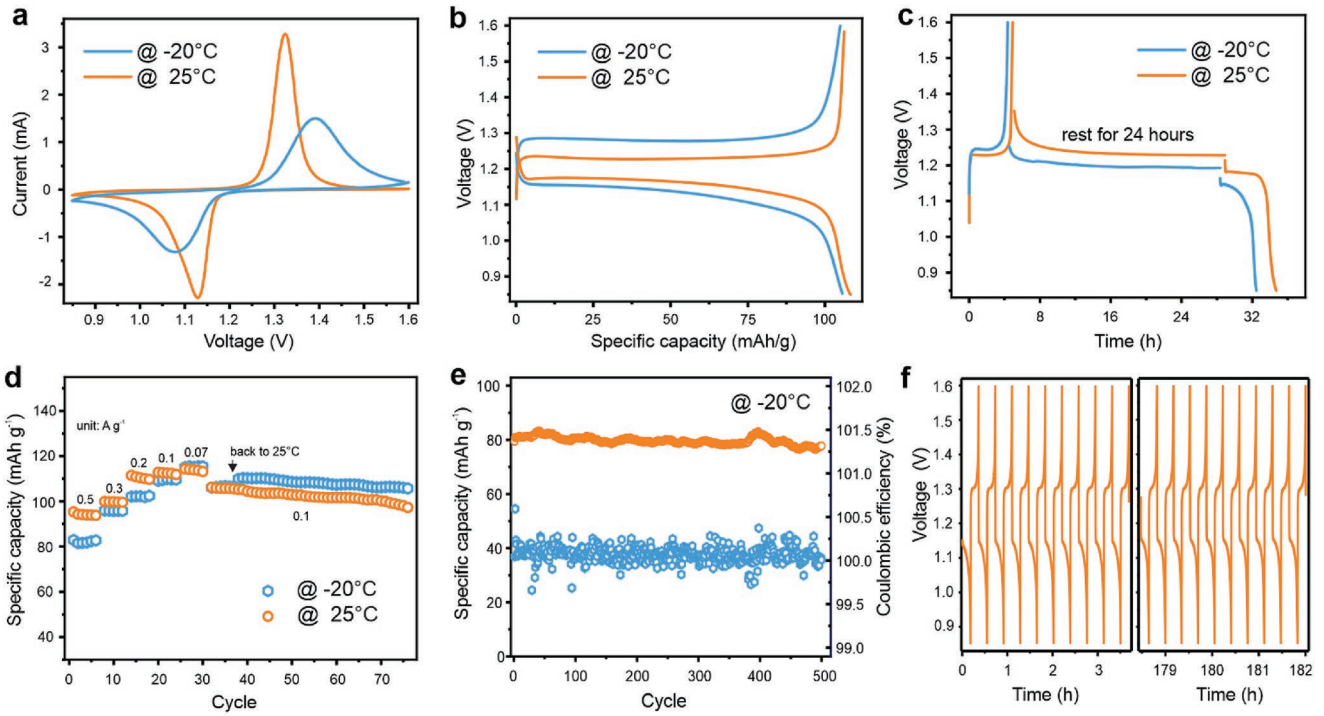

Figure 4. a) CV curves (5 mV s^{-1}) and b) charge–discharge profiles (0.1 A g^{-1}) of the Zn/$LiFePO_4$ hybrid battery at −20 and 25 °C. c) Discharge profile (0.1 A g^{-1}) of the Zn/$LiFePO_4$ after charging and storing at −20 and 25 °C for 24 h. d) Rate performance of the Zn/$LiFePO_4$ at −20 and 25 °C. e) Cycling stability (0.5 A g^{-1}) and f) magnified charge–discharge profiles of the Zn/$LiFePO_4$ at −20 °C.

metal substrate, the Li^+ ions are also absorbed. Consequently, the underpotential hydrogen evolution is prohibited and so is the $Zn(OH)_2$. Moreover, the adsorbed Li^+ guides the peculiar growth of the Zn, which creates the "porosity" that is beneficial for the mass transfer.

To demonstrate the low temperature durability and highly reversible zinc plating–stripping of ZL-PAAm in actual full batteries, $LiFePO_4$ is used as the cathode to couple with Zn in ZL-PAAm. In such hybrid batteries (Zn/$LiFePO_4$), the well-established Li^+ intercalation-deintercalation occurs at $LiFePO_4$ in a highly reversible way. At the same time, Zn plating and stripping occurs at the Zn anode. **Figure 4**a shows the CV curves of the full battery at −20 and at 25 °C (room temperature). A single pair of redox peaks is observed, which is consistent with the typical phase-transition between $LiFePO_4$ and $FePO_4$. The CV curve at −20 °C shows a decrease in peak current and increase in voltage gap between the redox peaks, indicating an inferior charge storage and slow kinetics at subzero temperatures. However, the highly reversible redox peaks are still observed at higher scan rates in CV curves measured at −20 °C (Figure S18, Supporting Information), indicating the energy storage ability can be well maintained in fast charge–discharge processes. In accordance with the CV curves, the charge–discharge profiles under the current density of 0.1 A g^{-1} (Figure 4b) show that the capacity slightly decreases from 106 to 104 mAh g^{-1} upon cooling down to −20 °C from room temperature. In addition, the voltage difference between charge and discharge plateaus becomes larger. The reduced discharge voltage results in the loss of energy density in practical applications. Prior to further exploration of the performance of the Zn/$LiFePO_4$ battery based on ZL-PAAm, the self-discharge, a typical challenge for batteries that directly use hydrogel as the electrolyte, is investigated. The assembled battery is charged under 0.1 A g^{-1} and discharged after 24-hour storage under −20 °C and at room temperature. As shown in Figure 4c, typical discharge profiles are observed at both temperatures. 100% and 94% of the original capacity are retained at room temperature and −20 °C, respectively. In addition, 100% capacity retention is achieved when discharging the Zn/$LiFePO_4$ battery at 1 A g^{-1} after being fully charged at 0.1 A g^{-1} and stored for 24 h (Figure S19, Supporting Information). All these results confirm that ZL-PAAm, as the quasi-solid-state electrolyte for the aqueous battery, functions well as the separator and prevents any parasitic reactions. Figure 4d shows the rate performance of the assembled battery. Obviously, the capacity decreases with increasing current density due to kinetic limitations. The degradation of capacity under high current densities is more serious at −20 °C, which is ascribed to the further limited kinetics at subzero temperatures. However, it is observed that the capacity shows only a small difference at low current density (e.g., 0.07 and 0.1 A g^{-1}) at −20 °C and room temperatures, indicating the good performance of the ZL-PAAm at subzero temperatures. It is noteworthy that the slight enhancement of the capacity is observed when the temperature recovers during the cycling. This could be explained by the repair of the electrode–electrolyte interface at subzero temperatures, which prolongs the cycling life for the battery.[54] The assembled aqueous battery can be cycled with both high stability and high Coulombic efficiency at −20 °C. At the current density of 0.5 A g^{-1}, an excellent stability with almost 100% capacity retention and 100% Coulombic efficiency

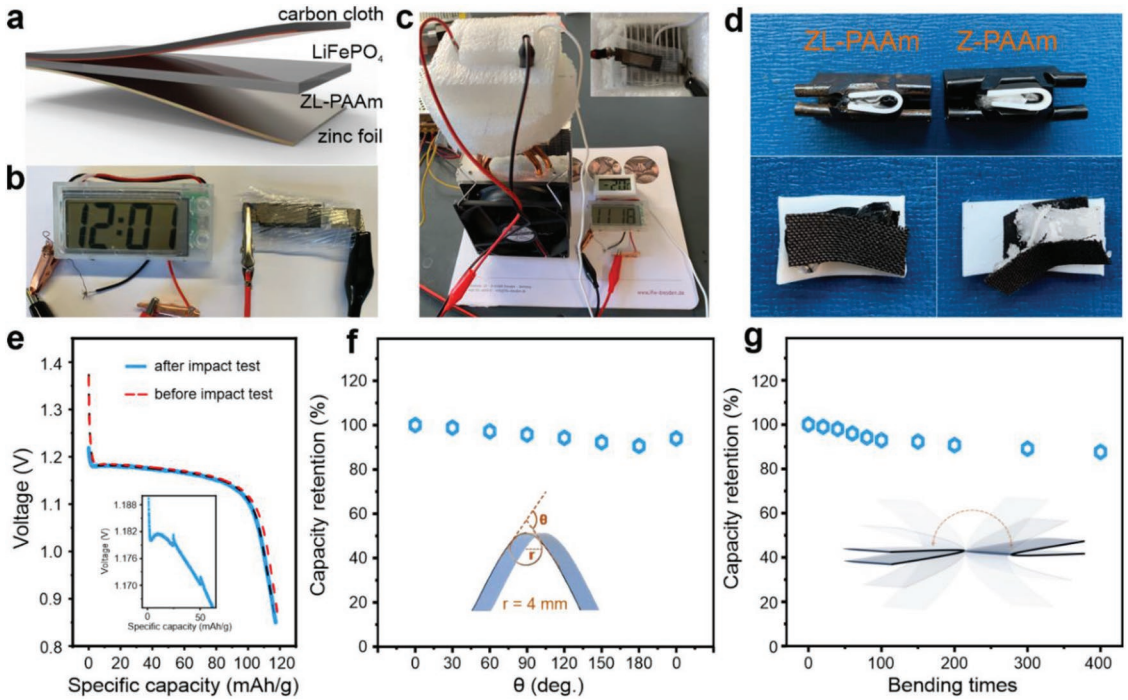

Figure 5. a) Scheme of the assembled flexible Zn/$LiFePO_4$ battery. Digital photographs of powered digital watch by the flexible Zn/$LiFePO_4$ battery at b) 25 °C and c) −20 °C. d) Digital photographs of the curved flexible Zn/$LiFePO_4$ battery storing at −20 °C for 24 h. e) Discharge curve of the flexible Zn/$LiFePO_4$ battery under repeated impact test. The inset shows the magnified region upon impact. Capacity retention of the flexible Zn/$LiFePO_4$ battery under f) different bending angles and g) bending times.

over 500 cycles are measured in Figure 4e. The charge–discharge profiles at the beginning and during the last cycles are displayed in Figure 4f. Apparently, both charge and discharge curves for the last cycles remain similar to the initial cycles, indicating the capacity achieved comes from the energy storage, not the consumption of charges due to parasitic reactions. This further demonstrates the excellent durability of the aqueous battery based on ZL-PAAm.

Targeted on practical applications, the flexible Zn/$LiFePO_4$ battery based on ZL-PAAm is assembled as illustrated in **Figure 5**a, in which the ZL-PAAm is sandwiched between a carbon cloth coated with $LiFePO_4$ and a thin zinc foil. Due to the negligible self-discharge, ZL-PAAm can simultaneously serve as the separator. The battery is sealed in a plastic bag to prevent water loss in ambient conditions and minimize any possible loss of flexibility caused by a rigid encapsulation. A digital watch can be easily powered by the flexible aqueous battery (Figure 5b). Moreover, the battery functions well even if stored at −20 °C as shown in Figure 5c. The stable interface between electrodes and the electrolyte is crucial for the reliable operation of the battery. For a flexible battery, the interface should be durable after mechanical deformations. Figure 5d shows the interface of the curved flexible Zn/$LiFePO_4$ battery after storing the device at −20 °C for 24 h. The ZL-PAAm does not freeze and the interface with electrodes maintains well. In contrast, the Z-PAAm is easily crushed due to the brittleness caused by the icing of the hydrogel. Moreover, electrodes are detached from the hydrogel, leading to the failure of the battery. Video S1 (Supporting Information) further shows the flexibility of the aqueous battery, which can be severely deformed with stable energy output. Moreover, the battery even can recover functionality after cutting as shown in Video S2 (Supporting Information). The short-circuit during the cutting is introduced by the metallic scissor. However, the quick recovery shows excellent resilience of the ZL-PAAm, which can prevent any short circuit. More rigorous tests are applied to the flexible Zn/$LiFePO_4$ battery to demonstrate its durability. Note that all the tests are carried out directly after storing the flexible aqueous battery at −20 °C for 24 h. In Figure 5e, we compare the discharging curve under periodic impact force. No capacity loss nor any short circuit are observed, demonstrating the high mechanical strength of the ZL-PAAm, which guarantees stable operation of the flexible Zn/$LiFePO_4$ battery. The inset in Figure 5e shows a magnified profile upon the impact, where we can only observe <5 mV fluctuation of the voltage. This confirms the durability of ZL-PAAm and excellent performance as the separator that prevents the short circuit. Video S3 (Supporting Information) further supports this claim as ultrastable voltage is observed under a repetitive hammering test. Figure 5f shows the capacity retention under different bending states. The flexible Zn/$LiFePO_4$ battery is stored at −20 °C for 24 h before each bending test. The radius for the bending is controlled down to 4 mm. More than 90% capacity retention is achieved at variant bending angles, confirming the high stability of the energy output with high flexibility. Furthermore, Figure 5g shows the capacity retention after multiple bending times. The flexible Zn/$LiFePO_4$ battery is stored at −20 °C for 24 h before every bending cycles. As illustrated in the inset of Figure 5g, one bending cycle corresponds to an ≈360° bending angle. Under such harsh testing condition, a small decay of the

capacity along with the increasing bending cycles is observed, which is attributed to the destruction of the interface between the electrode and ZL-PAAm. However, >80% capacity retention is still achieved by the flexible aqueous battery after 400 bending cycles. Moreover, during this bending test, the flexible Zn/$LiFePO_4$ battery has been repeatedly stored for ten times at –20 °C for 24 h. Apparently, 400 bending cycles and 10 repeated freezing processes mimic a very harsh environment for the operation of the flexible Zn/$LiFePO_4$ battery. Nevertheless, the high capacity retention demonstrates the outstanding durability under harsh operation environment. All in all, the flexible Zn/$LiFePO_4$ battery exhibits stable performance under different mechanical deformations after the freezing process, which is attributed to the excellent mechanical properties of ZL-PAAm over a wide temperature range and stable interface between electrodes and ZL-PAAm at subzero temperatures.

3. Conclusion

In conclusion, the supporting hydrated cation, Li^+, enables two unique properties for the PAAm hydrogel that are otherwise unavailable for single cation, Zn^{2+}, based PAAm hydrogel. The cooperative hydration of Zn^{2+} and Li^+ lowers the freezing temperature of the hydrogel. As a result, basic merits of hydrogels, high toughness, elasticity and ion transportation, are well preserved at subzero temperatures. Moreover, the cooperative adsorption of Li^+ effectively suppresses the underpotential hydrogen evolution. Thereby, the formation of $Zn(OH)_2$ and ZnO caused by the local rise of the pH due to the hydrogen evolution is prohibited. As a result, high reversibility of the Zn anode in ZL-PAAm is achieved. The flexible Zn/$LiFePO_4$ battery using ZL-PAAm as the electrolyte delivers a superb capacity retention of 98% upon cooling down to –20 °C from room temperature. Moreover, near 100% capacity is retained after 500 cycles at –20 °C with a Coulombic efficiency of >99.5%. In addition to the excellent energy storage performance at subzero temperatures, the mechanical durability is perfectly maintained after storing the flexible Zn/$LiFePO_4$ battery at –20 °C for 24 h. The fundamental understanding of the function of cooperative hydrated cations on antifreezing hydrogel and highly reversible zinc anode paves the way to the development of hydrogels for flexible aqueous batteries with low cost, high safety, durable mechanical properties, and high performance over a wide temperature range.

4. Experimental Section

Materials: Acrylamide, ammonium persulfate, *N,N′*-methylenebis(acrylamide), lithium chloride, lithium sulfate, zinc sulfate, zinc chloride, carbon black, polyvinylidene fluoride, and Zn foils were purchased from Sigma-Aldrich. $LiFePO_4$ was purchased from MTI corporation. The carbon cloth is purchased from CoTech Co., Ltd.

Preparation of PAAm-Based Hydrogel: 6 g acrylamide was dissolved in 40 mL deionized water, followed by the addition of 30 mg ammonium persulfate and 4 mg *N,N′*-methylenebis(acrylamide). The solution was under rigorous stirring until it became clear. Afterward, the prepared solution was injected into rubber molds and covered with a glass plate. The sample was kept at 70 °C for 3 h to allow complete polymerization. Subsequently, the samples were taken out of the molds and were directly used for testing. For the Z-PAAm and ZL-PAAm, the deionized water was replaced by the 2 mol L^{-1} $ZnSO_4$ and the mixture solution (2 mol L^{-1} $ZnSO_4$ and 1 mol L^{-1} LiCl), respectively.

Fabrication of the Zn/$LiFePO_4$ Battery: The $LiFePO_4$ electrode was prepared by mixing $LiFePO_4$ powders, carbon black and PVDF in a weight ratio of 7:2:1 by *N*-methyl-2-pyrrolidone, then casting the slurry on carbon cloth. After drying at 120 °C in vacuum for 12 h, the positive electrode with 2 mg cm^{-2} $LiFePO_4$ was achieved. The prepared positive electrode was coupled with Zn foil using ZL-PAAm as the electrolyte and separator. Afterward, the assembled battery was packaged in a plastic bag.

Characterization: Raman spectra of hydrogels were collected through LabRAM HR Evolution, HORIBA Scientific (wavelength of 442 nm). The dynamic mechanical analysis and tensile test were performed on EPLEXOR 500N (Gabo/Netzsch) and Z3 microtensile test machine (Grip-Engineering Thümler GmbH), respectively. The rheological properties of hydrogels were investigated with a stress-controlled bulk rheometer (Anton Paar MCR501). The morphology of cycled Zn foil was characterized by SEM (FESEM, DSM982 Gemini). XRD tests were performed on X'Pert PRO MPD, Philips (Co Kα radiation, $\lambda = 1.5418$ Å). Zn/Zn symmetric cells and Zn/Pt asymmetric cells are used for plating–stripping tests. Plating–stripping profiles and galvanostatic charge–discharge profiles were taken from the battery test system (Arbin 2000). CV curves and impedance spectra were measured by an electrochemical workstation (MULTIAUTOLAB/M101, Metrohm Autolab).

Supporting Information

Supporting Information is available from the Wiley Online Library or from the author.

Acknowledgements

M.Z. and X.W. contributed equally to this work. X.W., H.T., L.L., and Y.L. acknowledge financial support from the China Scholarship Council (CSC). Thanks to Dr. Lei Dong and Dr. Yang Huang for their support in NMR measurements.

Conflict of Interest

The authors declare no conflict of interest.

Keywords

antifreezing hydrogels, flexible aqueous batteries, freezing point depression, highly reversible zinc anodes, mechanical robustness

Received: September 2, 2019
Revised: October 16, 2019
Published online:

[1] H. Li, Z. Tang, Z. Liu, C. Zhi, *Joule* **2019**, *3*, 613.
[2] D. Chen, Z. Lou, K. Jiang, G. Shen, *Adv. Funct. Mater.* **2018**, *28*, 1805596.
[3] H. Cha, J. Kim, Y. Lee, J. Cho, M. Park, *Small* **2018**, *14*, 1702989.
[4] P. Yu, Y. Zeng, H. Zhang, M. Yu, Y. Tong, X. Lu, *Small* **2019**, *15*, 1804760.
[5] J. Chang, J. Shang, Y. Sun, L. K. Ono, D. Wang, Z. Ma, Q. Huang, D. Chen, G. Liu, Y. Cui, Y. Qi, Z. Zheng, *Nat. Commun.* **2018**, *9*, 4480.

[6] L. Liu, M. Zhu, S. Huang, X. Lu, L. Zhang, Y. Li, S. Wang, L. Liu, Q. Weng, O. G. Schmidt, *J. Mater. Chem. A* **2019**, *7*, 14097.
[7] H. Li, C. Han, Y. Huang, Y. Huang, M. Zhu, Z. Pei, Q. Xue, Z. Wang, Z. Liu, Z. Tang, Y. Wang, F. Kang, B. Li, C. Zhi, *Energy Environ. Sci.* **2018**, *11*, 941.
[8] F. Wan, L. Zhang, X. Dai, X. Wang, Z. Niu, J. Chen, *Nat. Commun.* **2018**, *9*, 1656.
[9] S. Luo, L. Xie, F. Han, W. Wei, Y. Huang, H. Zhang, M. Zhu, O. G. Schmidt, L. Wang, *Adv. Funct. Mater.* **2019**, *29*, 1901336.
[10] L. Perera, M. L. Berkowitz, *J. Phys. Chem.* **1993**, *97*, 13803.
[11] X. P. Morelle, W. R. Illeperuma, K. Tian, R. Bai, Z. Suo, J. J. Vlassak, *Adv. Mater.* **2018**, *30*, 1801541.
[12] Y. Bai, B. Chen, F. Xiang, J. Zhou, H. Wang, Z. Suo, *Appl. Phys. Lett.* **2014**, *105*, 151903.
[13] X. F. Zhang, X. Ma, T. Hou, K. Guo, J. Yin, Z. Wang, L. Shu, M. He, J. Yao, *Angew. Chem., Int. Ed.* **2019**, *58*, 7366.
[14] Q. Rong, W. Lei, L. Chen, Y. Yin, J. Zhou, M. Liu, *Angew. Chem., Int. Ed.* **2017**, *56*, 14159.
[15] F. Mo, G. Liang, Q. Meng, Z. Liu, H. Li, J. Fan, C. Zhi, *Energy Environ. Sci.* **2019**, *12*, 706.
[16] L. Guan, S. Yan, X. Liu, X. Li, G. Gao, *J. Mater. Chem. B* **2019**, *7*, 5230.
[17] D. Kundu, B. D. Adams, V. Duffort, S. H. Vajargah, L. F. Nazar, *Nat. Energy* **2016**, *1*, 16119.
[18] H. Li, L. Ma, C. Han, Z. Wang, Z. Liu, Z. Tang, C. Zhi, *Nano Energy* **2019**, *62*, 550.
[19] M. Song, H. Tan, D. Chao, H. J. Fan, *Adv. Funct. Mater.* **2018**, *28*, 1802564.
[20] G. Fang, J. Zhou, A. Pan, S. Liang, *ACS Energy Lett.* **2018**, *3*, 2480.
[21] J. Ming, J. Guo, C. Xia, W. Wang, H. N. Alshareef, *Mater. Sci. Eng., R* **2019**, *135*, 58.
[22] H. Pan, Y. Shao, P. Yan, Y. Cheng, K. S. Han, Z. Nie, C. Wang, J. Yang, X. Li, P. Bhattacharya, K. T. Mueller, J. Liu, *Nat. Energy* **2016**, *1*, 16039.
[23] A. Gomes, M. I. da Silva Pereira, *Electrochim. Acta* **2006**, *52*, 863.
[24] A. Gomes, M. I. Da Silva Pereira, *Electrochim. Acta* **2006**, *51*, 1342.
[25] D. S. Baik, D. J. Fray, *J. Appl. Electrochem.* **2001**, *31*, 1141.
[26] F. Wang, O. Borodin, T. Gao, X. Fan, W. Sun, F. Han, A. Faraone, J. A. Dura, K. Xu, C. Wang, *Nat. Mater.* **2018**, *17*, 543.
[27] X. Wu, Y. Xu, C. Zhang, D. P. Leonard, A. Markir, J. Lu, X. Ji, *J. Am. Chem. Soc.* **2019**, *141*, 6338.
[28] C. Y. Chen, K. Matsumoto, K. Kubota, R. Hagiwara, Q. Xu, *Adv. Energy Mater.* **2019**, *9*, 1900196.
[29] K. J. Tielrooij, N. Garcia-Araez, M. Bonn, H. J. Bakker, *Science* **2010**, *328*, 1006.
[30] M. Baumgartner, R. J. Bakker, *Mineral. Petrol.* **2009**, *95*, 1.
[31] X. Wu, W. Lu, W. Ou, M. C. Caumon, J. Dubessy, *J. Raman Spectrosc.* **2017**, *48*, 314.
[32] I. Duričković, M. Marchetti, R. Claverie, P. Bourson, J. M. Chassot, M. D. Fontana, *Appl. Spectrosc.* **2010**, *64*, 853.
[33] R. Buchner, T. Chen, G. Hefter, *J. Phys. Chem. B* **2004**, *108*, 2365.
[34] E. Pluhařová, P. E. Mason, P. Jungwirth, *J. Phys. Chem. A* **2013**, *117*, 11766.
[35] M. Hartmann, T. Clark, R. Van Eldik, *J. Am. Chem. Soc.* **1997**, *119*, 7843.
[36] J. D. Smith, R. J. Saykally, P. L. Geissler, *J. Am. Chem. Soc.* **2007**, *129*, 13847.
[37] M. Ahmed, V. Namboodiri, A. K. Singh, J. A. Mondal, *J. Chem. Phys.* **2014**, *141*, 164708.
[38] R. L. Wong, E. R. Williamsm, *J. Phys. Chem. A* **2003**, *107*, 10976.
[39] M. K. Gupta, R. Bansil, *J. Polym. Sci., Polym. Phys. Ed.* **1981**, *19*, 353.
[40] N. Dubouis, C. Park, M. Deschamps, S. Abdelghani-Idrissi, M. Kanduc, A. Colin, M. Salanne, J. Dzubiella, A. Grimaud, B. Rotenberg, *ACS Cent. Sci.* **2019**, *5*, 640.
[41] R. Bansil, M. K. Gupta, *Ferroelectrics* **1980**, *30*, 63.
[42] W. Wieczorek, J. R. Stevens, *Polymer* **1997**, *38*, 2057.
[43] W. Liu, S. W. Lee, D. Lin, F. Shi, S. Wang, A. D. Sendek, Y. Cui, *Nat. Energy* **2017**, *2*, 17035.
[44] P. Pissis, A. Kyritsis, *Solid State Ionics* **1997**, *97*, 105.
[45] M. Zhu, Z. Wang, H. Li, Y. Xiong, Z. Liu, Z. Tang, Y. Huang, A. L. Rogach, C. Zhi, *Energy Environ. Sci.* **2018**, *11*, 2414.
[46] T. Boiadjieva, M. Monev, A. Tomandl, H. Kronberger, G. Fafilek, *J. Solid State Electrochem.* **2009**, *13*, 671.
[47] N. Uekawa, R. Yamashita, Y. J. Wu, K. Kakegawa, *Phys. Chem. Chem. Phys.* **2004**, *6*, 442.
[48] S. Jiao, L. Xu, K. Hu, J. Li, S. Gao, D. Xu, *J. Phys. Chem. C* **2010**, *114*, 269.
[49] B. D. Adams, J. Zheng, X. Ren, W. Xu, J. G. Zhang, *Adv. Energy Mater.* **2018**, *8*, 1702097.
[50] E. Herrero, L. J. Buller, H. D. Abruña, *Chem. Rev.* **2001**, *101*, 1897.
[51] F. Hernandez, H. Baltruschat, *J. Solid State Electrochem.* **2007**, *11*, 877.
[52] S. Taguchi, A. Aramata, *J. Electroanal. Chem.* **1995**, *396*, 131.
[53] H. Yan, J. Downes, P. J. Boden, S. J. Harris, *J. Electrochem. Soc.* **1996**, *143*, 1577.
[54] J. Zhao, K. K. Sonigara, J. Li, J. Zhang, B. Chen, J. Zhang, S. S. Soni, X. Zhou, G. Cui, L. Chen, *Angew. Chem., Int. Ed.* **2017**, *56*, 7871.